Conf-9010283--3

# CALOR89: Calorimetry Analysis and Benchmarking†

CONF-9010283--3

DE91 006604

T. A. Gabriel, R. G. Alsmiller, Jr., B. L. Bishop and C. Y. Fu
Oak Ridge National Laboratory

T. Handler
University of Tennessee

J. K. Panzkkal and J. Proudfoot
Argonne National Laboratory

L. Cremaldi, B. Moore, and J. J. Reidy
University of Mississippi

Paper presented at the
International Conference on
Calorimetry in High Energy Physics
October 29-November 1, 1990
Batavia, Illinois 60510



Prepared by the
OAK RIDGE NATIONAL LABORATORY
Oak Ridge, Tennessee 37831
managed by
MARTIN MARIETTA ENERGY SYSTEMS, INC.
for the
U.S. DEPARTMENT OF ENERGY
under contract DE-AC05-84OR21400



† Managed by Martin Marietta Energy Systems, Inc. under Contract No. DE-AC05-84OR21400 for the U.S. Department of Energy.

# CALOR89: Calorimetry Analysis and Benchmarking

T. A. Gabriel, R. G. Alsmiller, B. L. Bishop and C. Y. Fu
Oak Ridge National Laboratory
Oak Ridge, Tennessee 37831/U.S.A.

T. Handler
University of Tennessee at Knoxville
Knoxville, Tennessee 37996-1200/U.S.A.

P. K. Job and J. Proudfoot
Argonne National Laboratory
Argonne, Illinois 60439/U.S.A.

L. Cremaldi, B. Moore and J. J. Reidy
University of Mississippi
University, Mississippi 38677/U.S.A.

ABSTRACT

The CALOR89 code system has been utilized for extensive calorimeter benchmarking and design calculations. Even though this code system has previously demonstrated its power in the design of calorimeters, major revisions in the form of better collision models and cross-section data bases have expanded its capabilities. The benchmarking has been done with respect to the ZEUS and DO calorimeters. For the most part, good agreement with experimental data has been obtained. The design calculations presented here were done for a variety of absorbers (depleted uranium, lead, and iron) of various thickness, for a given scintillator thickness and for a fixed absorber thickness using various thickness for the scintillator. These studies indicate that a compensating calorimeter can be built using depleted uranium or lead as the absorber, whereas a purely iron calorimeter would be non-compensating. One possibly major problem exists with the depleted uranium calorimeter due to the large number of neutrons produced and due to the large capture cross-section of uranium. These captured neutrons will produce a signal in the scintillator due to secondary gamma rays for many hundreds of nanoseconds and this may contribute substantially to background noise and pile up.

## 1. Introduction

During the past ten years, substantial progress has been made in the understanding of the physics of calorimeters[1]. This progress included the reason depleted uranium-liquid argon calorimeters are not compensating, the importance of hydrogen in the active media, especially for calorimeters utilizing large $Z$ absorbers, the physics behind the electromagnetic sampling inefficiency and its effect on compensation, and in general, the sensitivity of geometry and material on the overall performance of these

important detectors in high energy physics. This new knowledge compiled with improved code systems will allow for a much improved design on calorimeters to be used at the Superconducting Super Collider (SSC).

Since the calorimeters that are going to be used at the SSC are going to be large and expensive, it would be prohibitive to build full-scale prototypes. Therefore, the only avenue open is to build small-scale prototypes that can be tested and to compare these experimental results to the output of simulation programs. These simulation programs can then be used to design the calorimeters once their accuracy has been established by benchmarking against existing data. The CALOR89 code system is the program used in this paper to analyze calorimeters, existing and proposed.

The CALOR89 code system has been utilized for extensive calorimeter benchmarking and design calculations. Even though this program has previously demonstrated its power in the design of calorimeters, major revisions in the form of better collision models and cross-section data bases have expanded its capabilities. The benchmarking has been done with respect to the ZEUS and DO calorimeters. For the most part, good agreement with experimental data has been obtained. The design calculations presented here were done for a variety of absorbers (depleted uranium, lead, and iron) of various thickness for a given scintillator thickness and for a fixed absorber thickness using various thickness for the scintillator. These studies indicate that a compensating calorimeter can be built using depleted uranium or lead as the absorber, whereas a purely iron calorimeter would be non-compensating. One possibly major problem exists with the depleted uranium calorimeter due to the large number of neutrons produced and due to the large capture cross-section of uranium. These captured neutrons will produce a signal in the scintillator due to secondary gamma rays for many hundreds of nanoseconds and this may contribute substantially to background noise and pileup.

Presented in the following sections are a description of CALOR89, some of the benchmarking results, and predictions on proposed calorimeters.

## 1. CALOR89

The CALOR89 code system (Fig. 1) consist of four primary programs, HETC88[2], SPECT89, EGS4[3], and MORSE[4] or MICAP[5], plus their ancillary programs. A final user written analysis program combines and analyzes results of the various codes.

HETC88 is used to generate and transport the hadronic particles through the calorimeter. HETC88 does the particle transport and generation in a three fold manner: 1) For energies less than 3 GeV, particles are generated by means of an intermediate-energy Intranuclear-Cascade and Evaporation Model[6]; 2) From 3 GeV to approximately 10 GeV, particle generation is done by means of a scaling model, 3) From 10 GeV upwards, particle generation is done by means of FLUKA[7] which

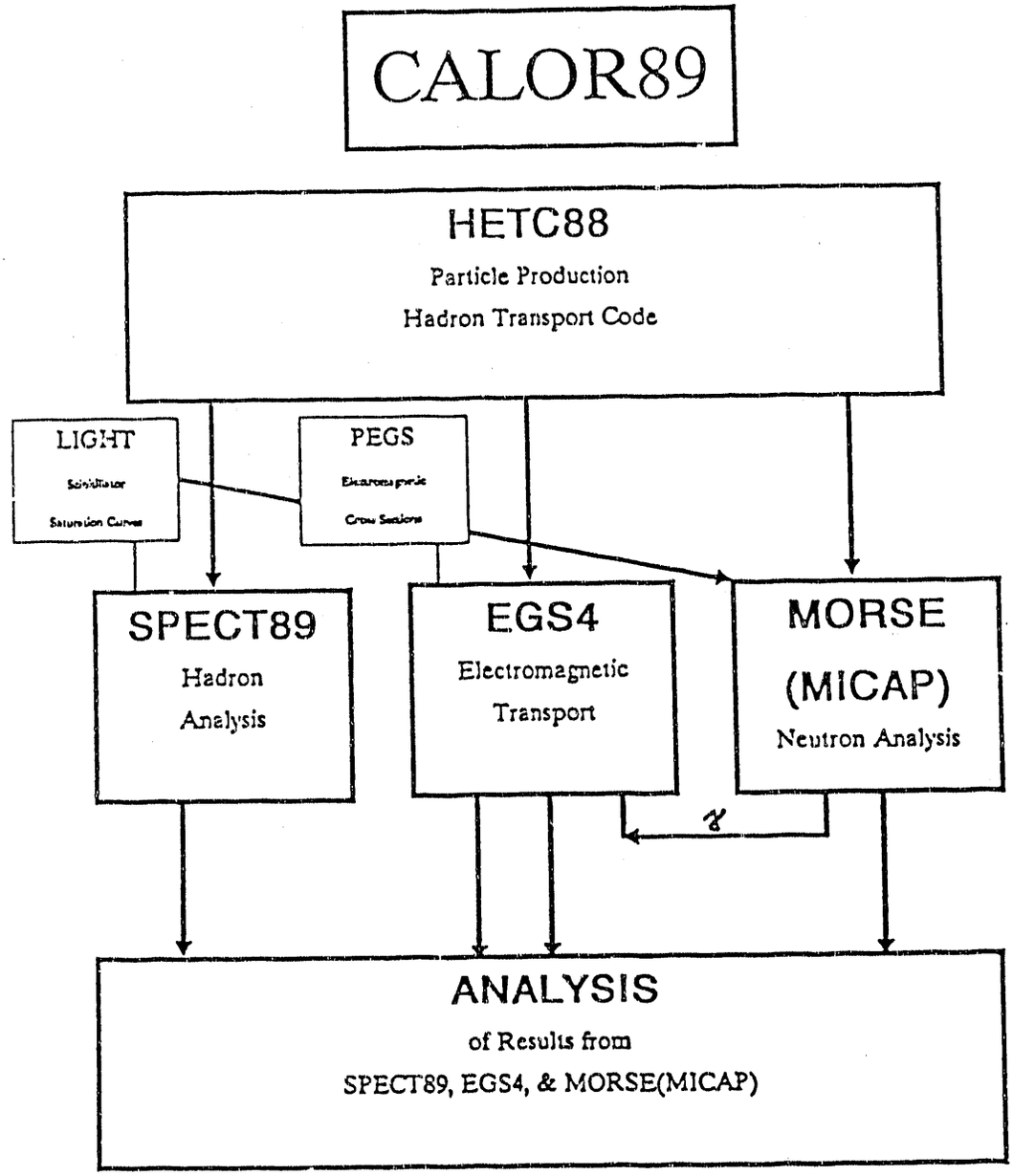


Fig. 1 CALOR89 code system.

uses a multi-chain fragmentation model. Inelastic nucleon hydrogen and charged-pion hydrogen collisions are done via the isobar model or a fragmentation model[2]. The boundary between the use of the Scaling Model and FLUKA is determined by a parameter, ESKALE, that is at the user's discretion. The energy at which the new collision physics is used is not yet determined nor is the method by which the conversion will take place. A discrete change is not desirable at this time, so possibly one model will be linearly phased out over a given energy range ($\approx$10 to 20 GeV) while the one is phased in. The decay of particles as well as the energy loss of charged particles due to ionization collisions is also included.

SPECT89 does the energy deposition analysis of the hadrons in the calorimeter. The ancillary program, LIGHT allows the user to take into account the non-linearity of the light pulse in the scintillator due to saturation effects within the active medium. This is done by use of Birk's law[8]. In the simulation of calorimeters and the comparison with the experimental test data it is imperative that saturation effects be taken into account. In Figure 2, the effects of saturation is shown. The simulation is for a slab calorimeter made from 4 mm lead sheet followed by a 1 mm sheet of scintillator repeated to a depth of 150 cm. As is seen in the figure, by not taking into account saturation effects, an overestimate is made of the hadronic signal, and therefore, a gross reduction in the compensation ratio. In general, ±8% variations in hadronic signal can result due to changes in scintillator saturation.

EGS4 is used for the transport and energy deposition analysis of electromagnetic particles in the calorimeter. The source data for EGS4 consists of direct photon production from hadron-nuclear collisions, photons from neutral pion decay, and electrons and positrons from muon decay. These are taken from the HETC88 analysis tape.

MORSE or MICAP is used to transport neutrons that are produced with energies less than 20 MeV and to generate the gamma rays from inelastic, fission and capture reactions. These subsequent gammas are then transported by EGS4. Both MORSE and MICAP have time dependence built into the code.

The programs SPECT89, EGS4, and MORSE (MICAP) do NOT explicitly incorporate many of the experimental details that are always there. These details include non-uniformity of light collection, electronic noise, pedestal cuts, material noise (natural fission noise), etc. These effects can be incorporated into the analysis parts of SPECT89, EGS4, and MORSE (MICAP) or some can be included during the final analysis.

Due to the accuracy of the CALOR89 code system and to the sensitivity of the calorimeter response to its size and material composition, minimum calculational approximations should be used. Many times the wrong answer has been obtained by trying to homogenize parts of the calorimetry, using incorrect cut offs or making the

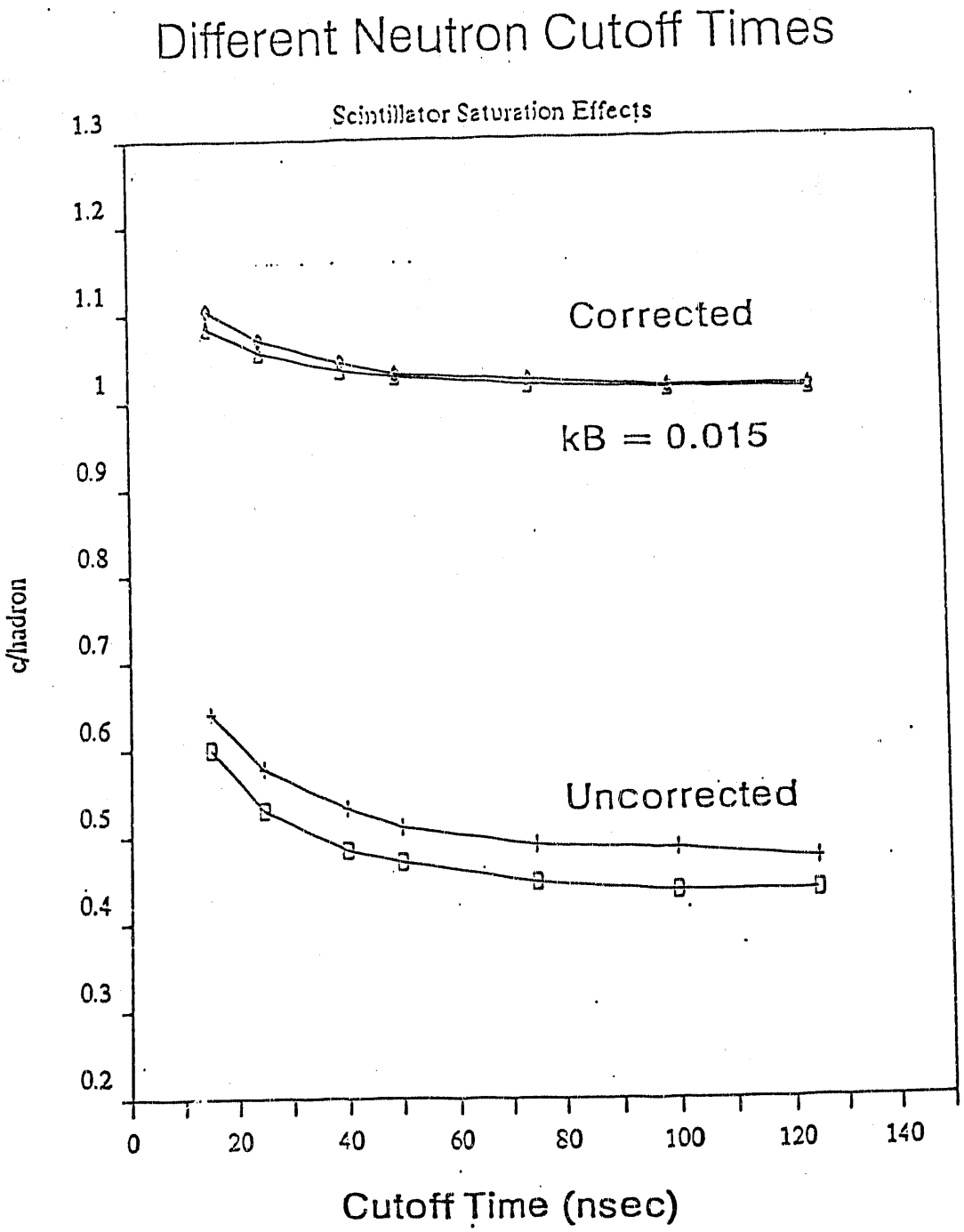


Fig. 2 Scintillator saturation effects - Lower curves represent uncorrected scintillator signals, while upper curves have been corrected for saturation effects.

calorimeter too large. Comparisons obtained with too many assumptions will not necessarily be exact. For example, consider the calculated data in Fig. 3 which gives the energy deposition in plastic scintillator for a sampling calorimeter. If the electron cut off energy is set too large the wrong answer is obtained. This type of error can lead to a wrong conclusion when, for example, a compensating calorimeter is trying to be designed. Sensitivity calculations should always be done to obtain the optimum value of input parameters for any code system. The parameters are generally problem dependent. Simulation codes are not perfect and demand experienced users if their full potential are to be realized.

## 3. Benchmarking Calculations

### 3.1 ZEUS

Preliminary results have been obtained from the CALOR89 code system for the ZEUS prototype lead-scintillator and depleted uranium-scintillator calorimeters[9-12]. These results are presented in Table 1.

| Table I | | |
|---|---|---|
| CALOR89 Benchmarking Data | | |
| ZEUS Compensation | | |
| 10 GeV $\pi^-$ | | |
| | Depleted Uranium-Scintillator | Lead-Scintillator |
| Thickness | 0.33/0.26 cm | 1.00/0.25 cm |
| Calculated | 1.01 ± 0.03 | 0.99 ± 0.08 |
| Experimental | 1.01 ± 0.04 | 1.05 ± 0.02 |

The slight difference between the lead data is not totally understood, but is under investigation. However, overall the agreement is very good. Comparison with the energy resolution is also very good.

### 3.2 DO

In a recent paper, experimental results were presented on the hadronic and electronic response of a uranium-liquid argon calorimeter module[13]. The module used was a hadronic section of the DO calorimeter and the quantities measured were the energy resolution, the electromagnetic to hadronic response ratio ($e/\pi$) and the

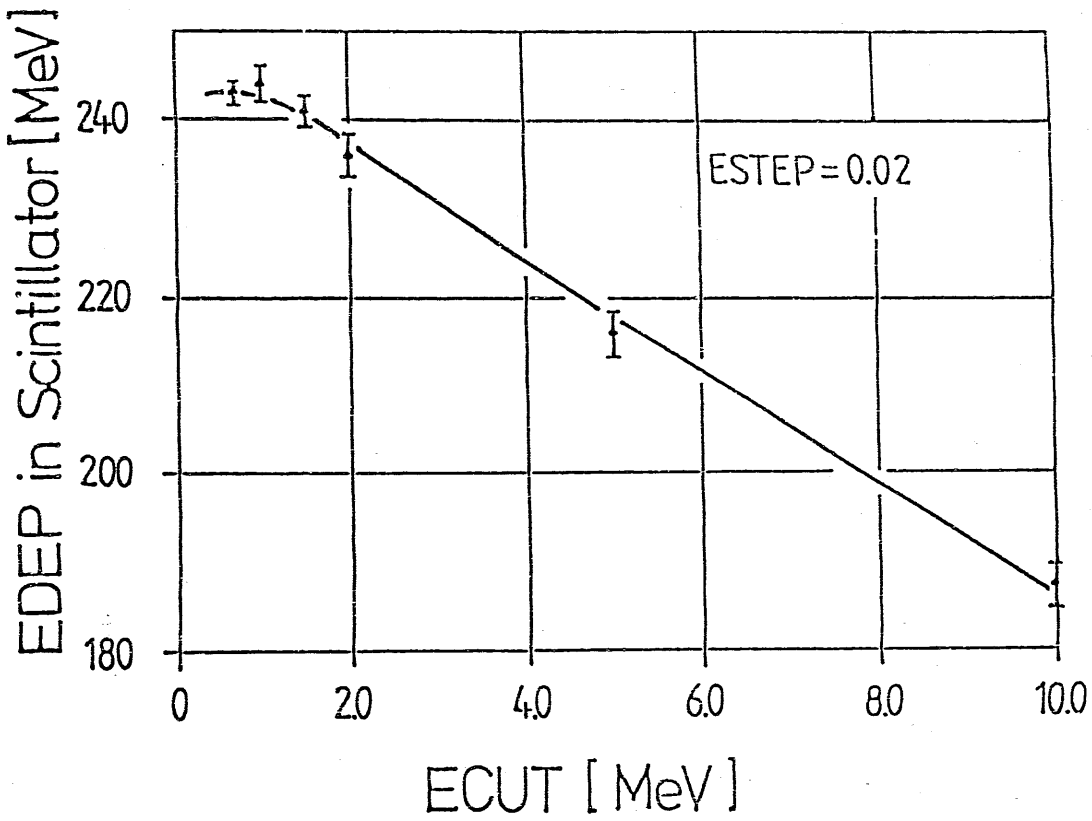


Fig. 3 Sensitivity of the energy deposition in plastic scintillator to the electron cut off energy.

longitudinal hadronic shower development. Experimental data was presented for incident particle energies of 25 to 150 GeV. Work is in progress to obtain comparisons between this experimental data and calculated results obtained with the CALOR89 computer code system.

The dimensions of the calorimeter module are given in detail in Ref. 13 and will not be repeated here. The calorimeter module is basically 6 mm uranium plates separated by 5.7 mm of liquid argon and G10 signal board. At the back of the module, the uranium is replaced by stainless steel. In the calculations, the module was modeled in rather complete detail using the combinatorial geometry routine included in CALOR89. Standard techniques were applied to make consistent the signals for the two different sections.

In Fig. 4, the calculated and measured integrated longitudinal shower containment for 25 GeV incident pions are compared as a function of thickness. The circles are taken from Ref. 13 and are the prediction of a parameterization. In the figure, both the calculated and experimental data have been normalized to agree with the parameterization at the largest thickness shown.

In Figs. 5(a) and 5(b), the measured fractional resolution is shown as a function of incident energy for electrons and pions. The solid curves are fits to the experimental data taken from Ref. 13. Calculated values for 25 GeV and 100 GeV incident pions and electrons are also shown. The two calculated values for incident pions corresponding to integration times of 50 ns and 250 ns (these times do not include charge collection time). The experimental values contain noise, and this same noise has been added to the calculated values for comparison purposes. The agreement between the calculated and experimental data is quite satisfactory. These experimental data points have been corrected for leakage, thereby, explaining the discrepancy at 100 GeV.

In Fig. 6, the measured hadronic-to-electromagnetic energy deposition ratio ($e/\pi$) is shown as a function of incident particle energy. Also shown are the calculated values for integration times of 50 ns and 250 ns. There is a noticeable difference between the results for the two integrations times and the longer time gives the better agreement with the experimental data. The experimental data was integrated over 1000 ns. In Fig. 7, the $e/\pi$ calculated ratio is given as a function of integration time out to 500 ns. As can be seen, the value of $e/\pi$ is still decreasing, but at an increasingly slower rate.

## 4. Design Calculations

A series of calculations to determine the sensitivity of the compensation and resolution characteristics of a prototypic calorimeter composed of various absorber

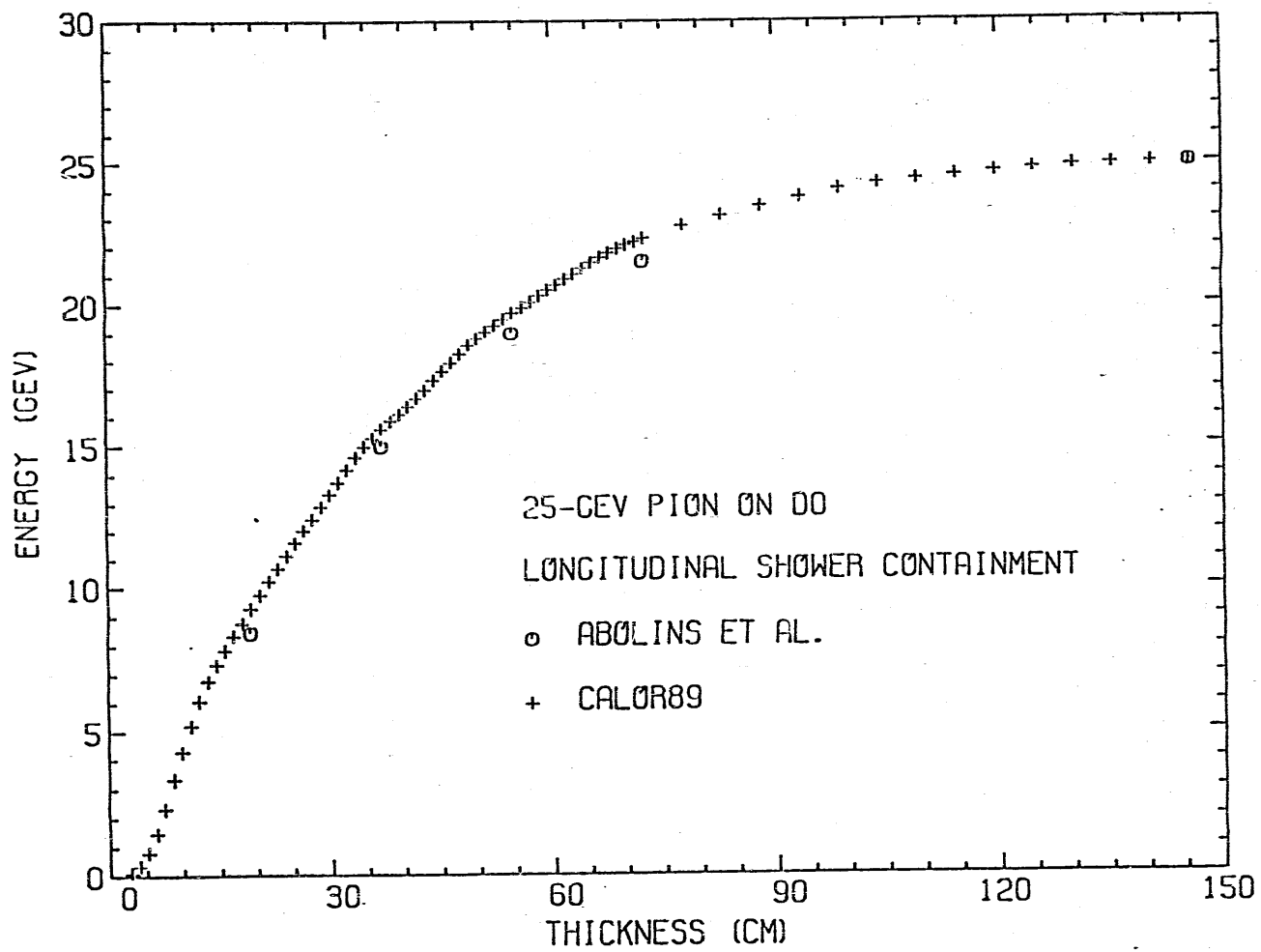


Fig. 4 Integrated shower containment for 25 GeV pion in the DO calorimeter as a function of depth.

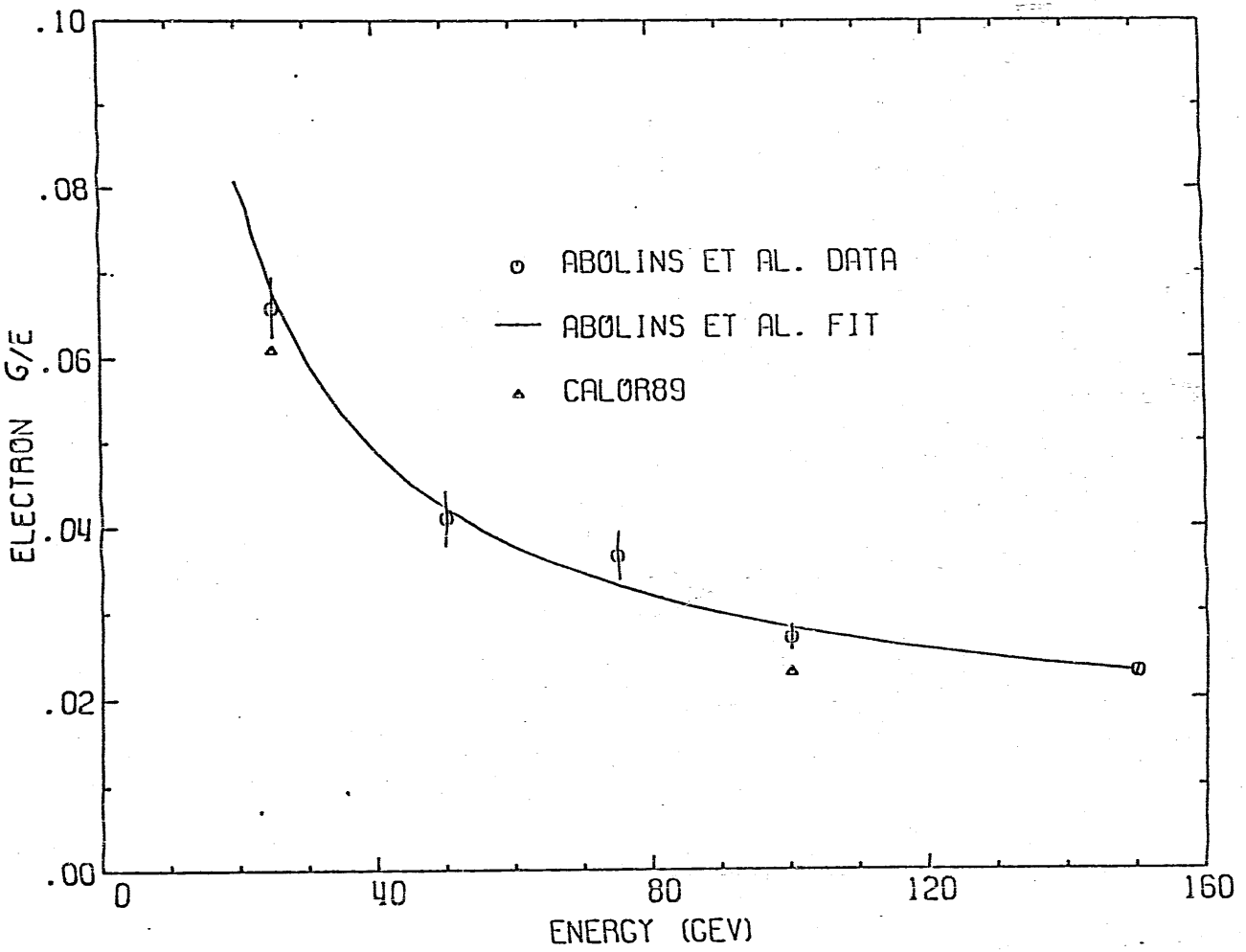


Fig. 5(a) Electron energy resolution for the DO calorimeter as a function of electron energy.

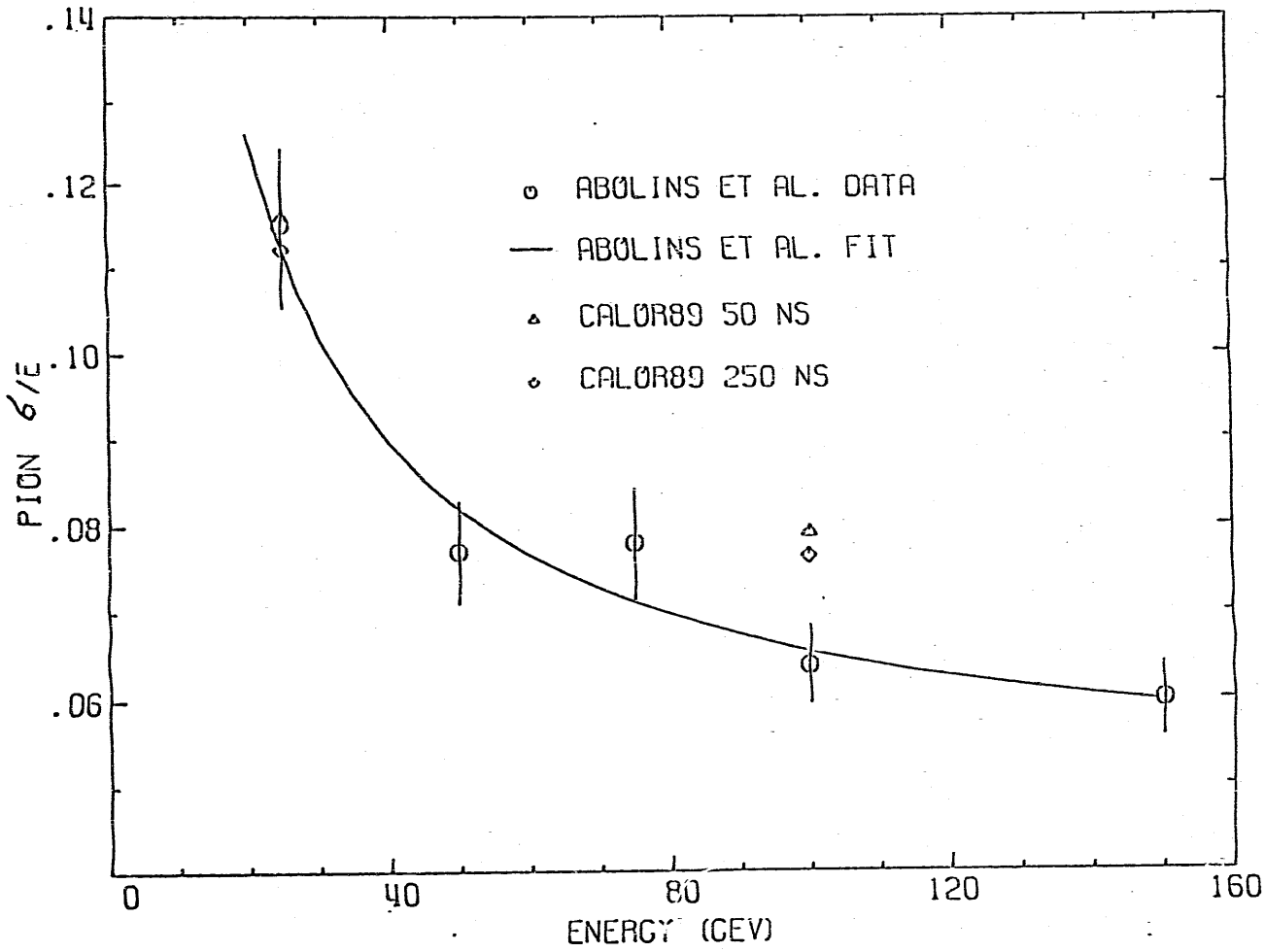


Fig. 5(b) Pion energy resolution for the DO calorimeter as a function of pion energy and integration time.

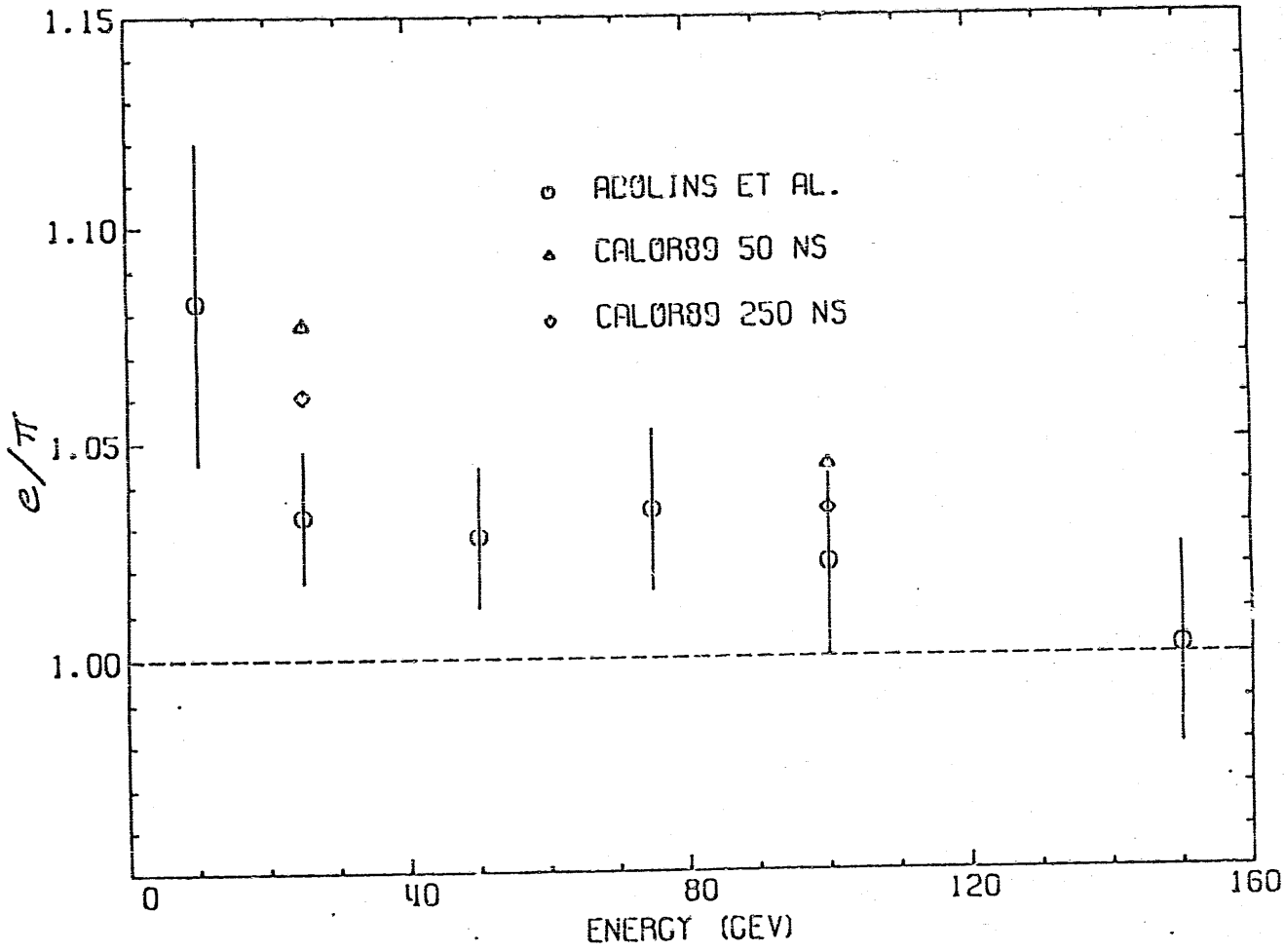


Fig. 6 Compensation Ratio ($e/\pi$) for the DO calorimeter as a function of energy.

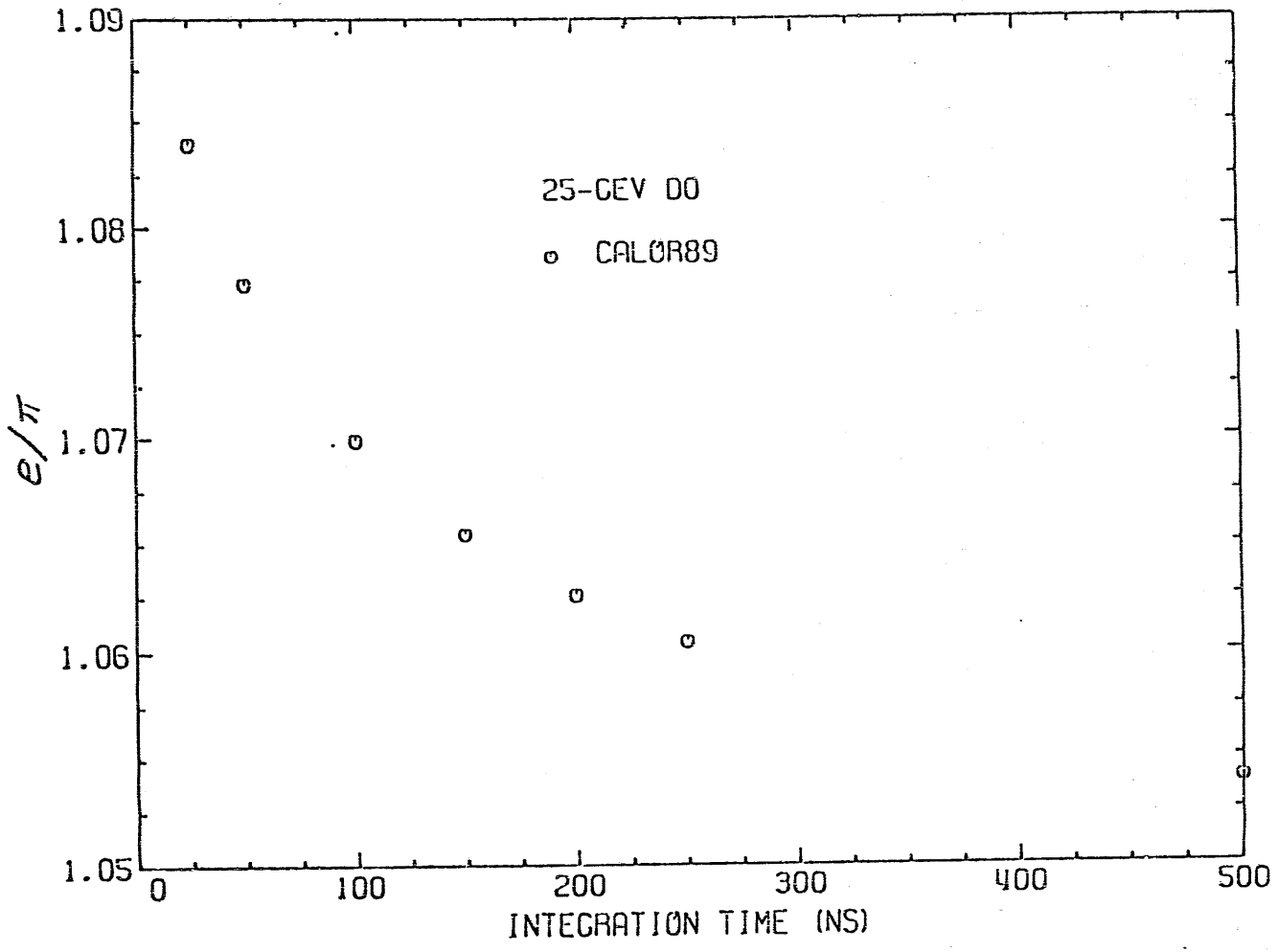


Fig. 7 Compensation Ratio ($e/\pi$) for the DO calorimeter at 25 GeV as a function of integration time.

materials (depleted uranium, lead, and iron) of various thicknesses (0.5, 1.0, 2.0, and 4.0 radiation length) in conjunction with various scintillator thicknesses (0.1, 0.25, 0.5, and 1.0 cm) have been carried out. The incoming particle used was a 10 GeV kinetic energy negative pion and a 10 Gev electron. Birk's constant for the scintillator saturation level was set at 0.0131 gm/cm$^2$/MeV. The calorimeter was 2 m by 2 m by 8 interaction lengths of absorber material. The complete matrix of absorber thicknesses and scintillator thicknesses was not explored. In one series of calculations, the scintillator thickness was fixed at 0.25 cm and the various absorber thicknesses were used. In another series of calculations, the absorber thickness was fixed at one radiation length and the scintillator thickness was varied. Various gate times were used in the low energy neutron and subsequent gamma analysis. The actual gate time has an uncertainty of approximately 5 - 10 nsec due to the fact that no timing is done in HETC88 or EGS4.

Presented in Fig. 8 are the compensation results at 10 GeV for the three absorbers as function of absorber thickness divided by scintillator thickness (Fig. 8(a)) when the scintillator was held fixed at 0.25 cm and as a function of scintillator thickness divided by absorber thickness (Fig. 8(b)) when the absorber was held fixed at 1.0 radiation lengths. The two curves for each of the absorber materials represent calculations done with ESKALE set at 5 GeV, the lower curve, and set at 15 GeV, the upper curve. The gate width used in the calculations was 48ns. For the iron and lead cases, this gate width is sufficient to collect the large majority of the signal. However, for the uranium case, this is not true due to the fact that uranium through fission processes produces additional neutrons and that uranium has a very large capture cross-section at energies less than 1 MeV. (See Fig. 9.) In a large calorimeter system and in a high luminosity environment, the produced gammas may yield a significant contribution to background noise and thus produce pileup problems. The experimental data points, even though they are from calorimeters not simulated by these calculations, are plotted to show that the calculations agree with the general trends. Most experimental results from uranium calorimeters do not show the effect demonstrated in Fig. 9. Their size allows for low energy neutron (< 1 MeV) leakage before capture. Also due to the large volume over which this signal is generated, part of this signal may be lost due to poor light or charge collection. Therefore, there signal would flatten out after ≈50-100 ns similar to the iron and lead results in Fig. 9. The iron experimental data point represents a "weighted" value. The unweighted value is $1.36 \pm 0.04$, which yields a more consistent trend with respect to the other experimental data.

In Fig. 8(a), the iron calculations show that there seems to be no strong dependence of the compensation on absorber thickness. There is a stronger dependence for the lead and uranium cases. This is due, in part, to the strong $Z$ dependence of the electromagnetic cross-sections. In Fig. 8(b), the curves have to approach each other as the scintillator thickness becomes sufficiently large to contain both the electromagnetic and hadronic cascade.

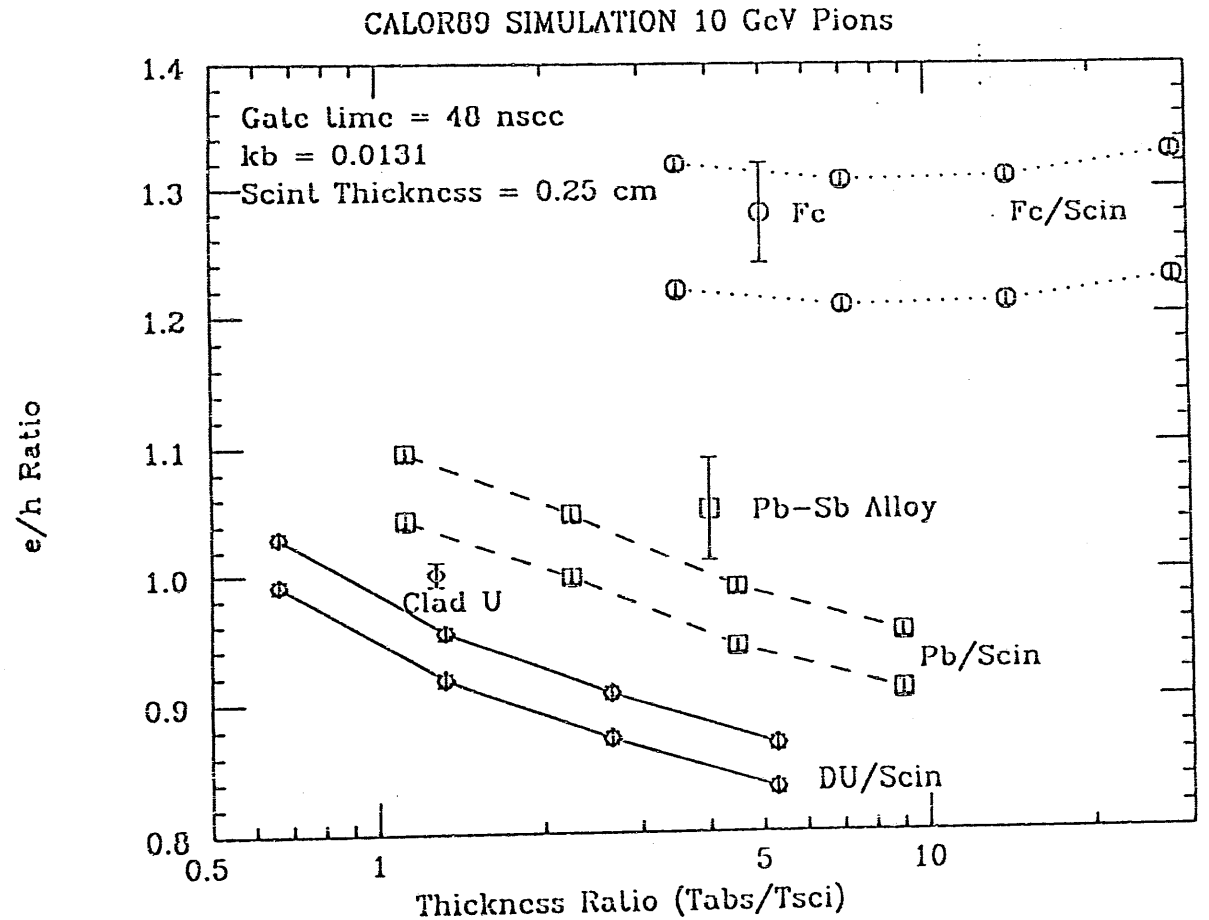


Fig. 8(a) The compensation ratio is shown as a function of absorber thickness divided by a fixed scintillator thickness.

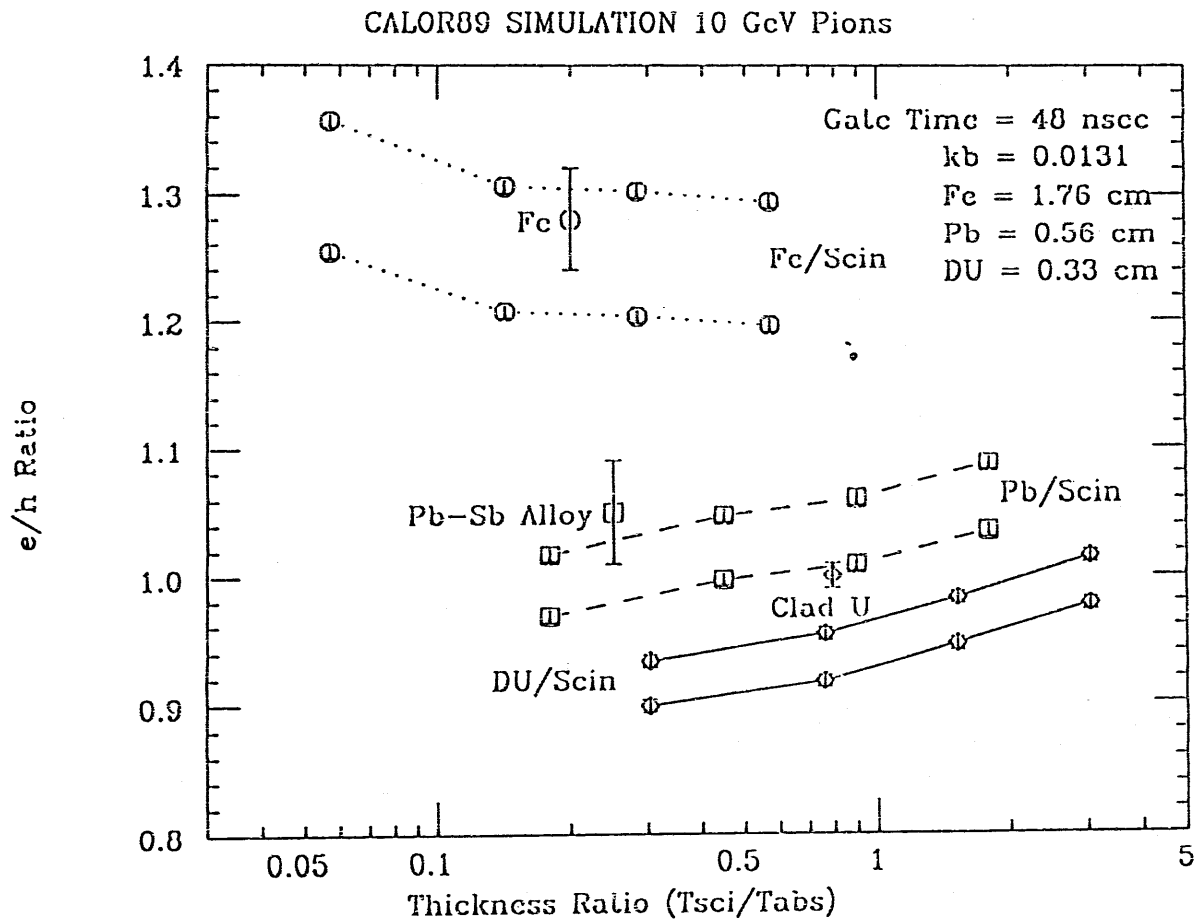


Fig. 8(b) The compensation ratio is shown as a function of scintillator thickness divided by a fixed thickness of absorber.

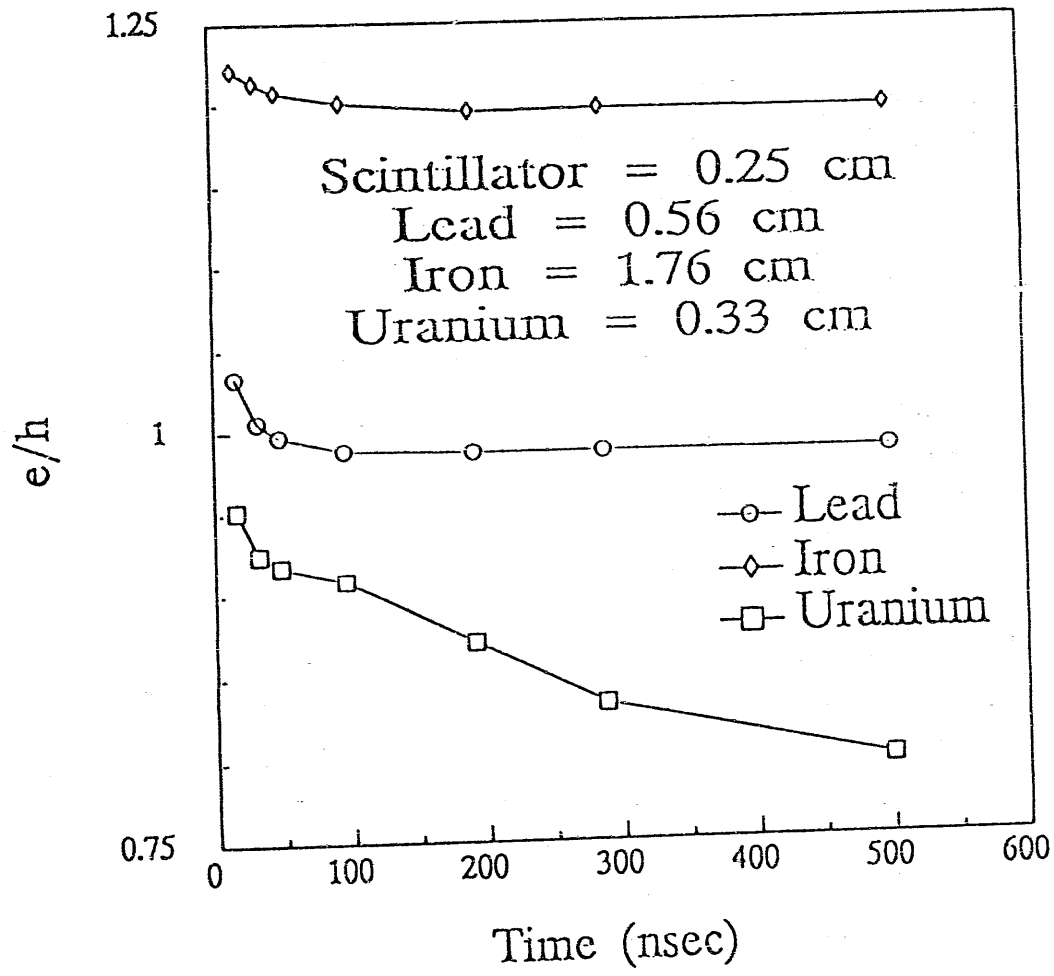


Fig. 9 Compensation as a function of integration time and passive absorber material (10 GeV $\pi^-$). The continued decrease for the uranium calorimeter is due to the size of the calorimeter, to the large number of neutrons, and to the large U capture cross-section.

In Fig. 10(a), the hadronic resolution is presented as a function of absorber thickness divided by the scintillator thickness which was held fixed at 0.25 cm and in Fig. 10(b) for scintillator thickness divided by absorber thickness which was held at 1.0 radiation lengths. Only the calculation done at an ESKALE 5 GeV is presented as the values for ESKALE at 15 GeV lie basically on top of the these values. The comparison with the uranium and lead resolution data appears quite good. It is felt that the disagreement between the iron calculation and the iron data point is probably due to the strong data cuts applied and to the lateral size of the calorimeter.

In Fig. 11, similar curves are presented for the electromagnetic resolution. The agreement between the calculations and the experimental data are again good except for the iron data point. As in the case of the Fe hadronic data point, it is felt that their experimental cuts are possibly the cause.

It has been suggested that by placing hydrogenous material on either side of a plastic scintillator in conjunction with an iron absorber, that such a calorimeter could be made compensating. Calculations utilizing CALOR89 indicate at 10 GeV at most a 5% improvement in the compensation characteristics. The calculations that were carried out were for an iron absorber of thickness 2.54 cm followed by 5 independent 0.2 cm thick plastic scintillators. This unit cell was repeated for 8 interaction lengths of iron. The results of these calculations are given in Figs. 12-14.

## 5. Summary

The CALOR89 code system has been used to compare with various calorimeter prototypes. In general, the agreement obtained has been satisfactory or discrepancies can be traced to experimental cuts, biases, leakage, etc. This code system has been used to generate preliminary design data for a variety of absorber, scintillator configurations. These results give general trends on the anticipated changes in the energy resolution and compensation characteristics.

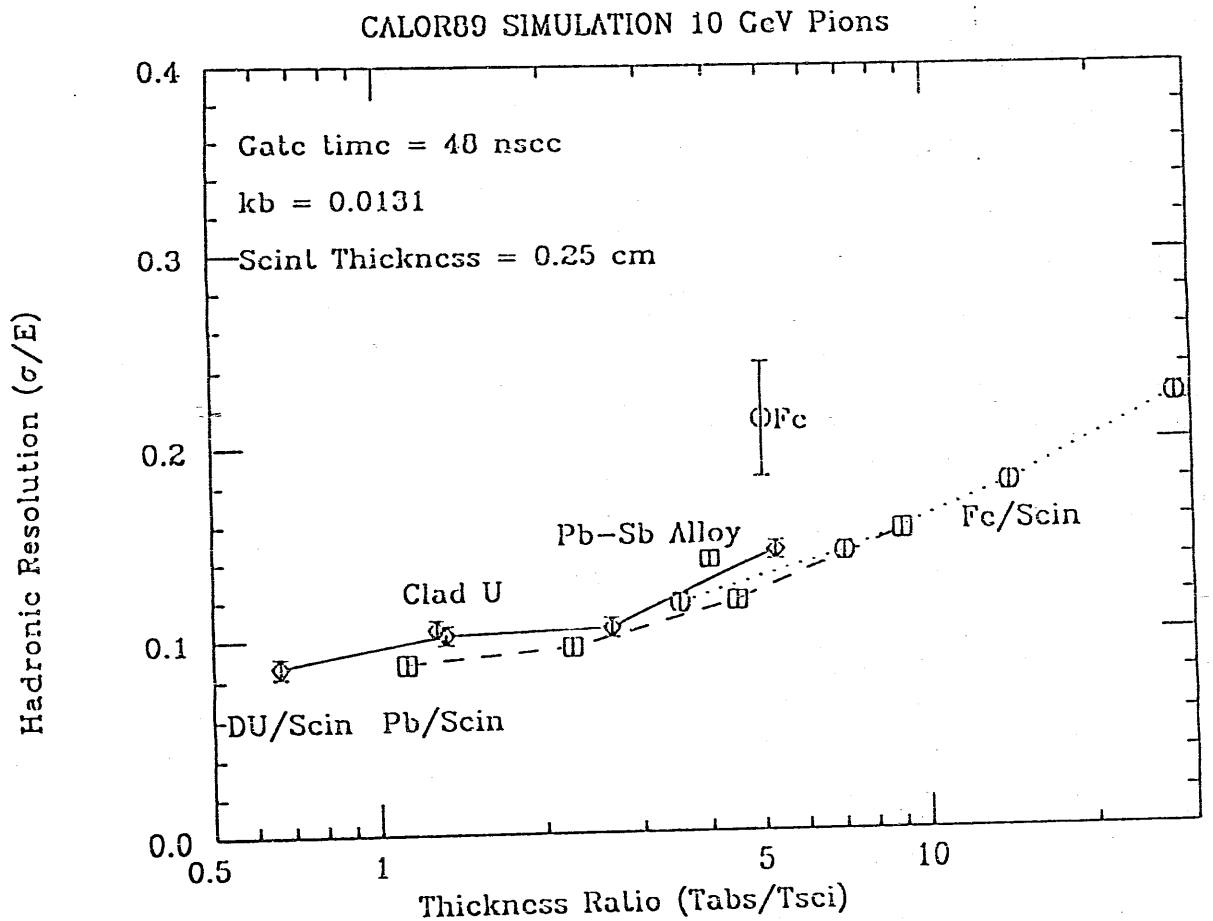


Fig. 10(a) Hadronic energy resolution as a function of absorber thickness divided by a fixed thickness of scintillator.

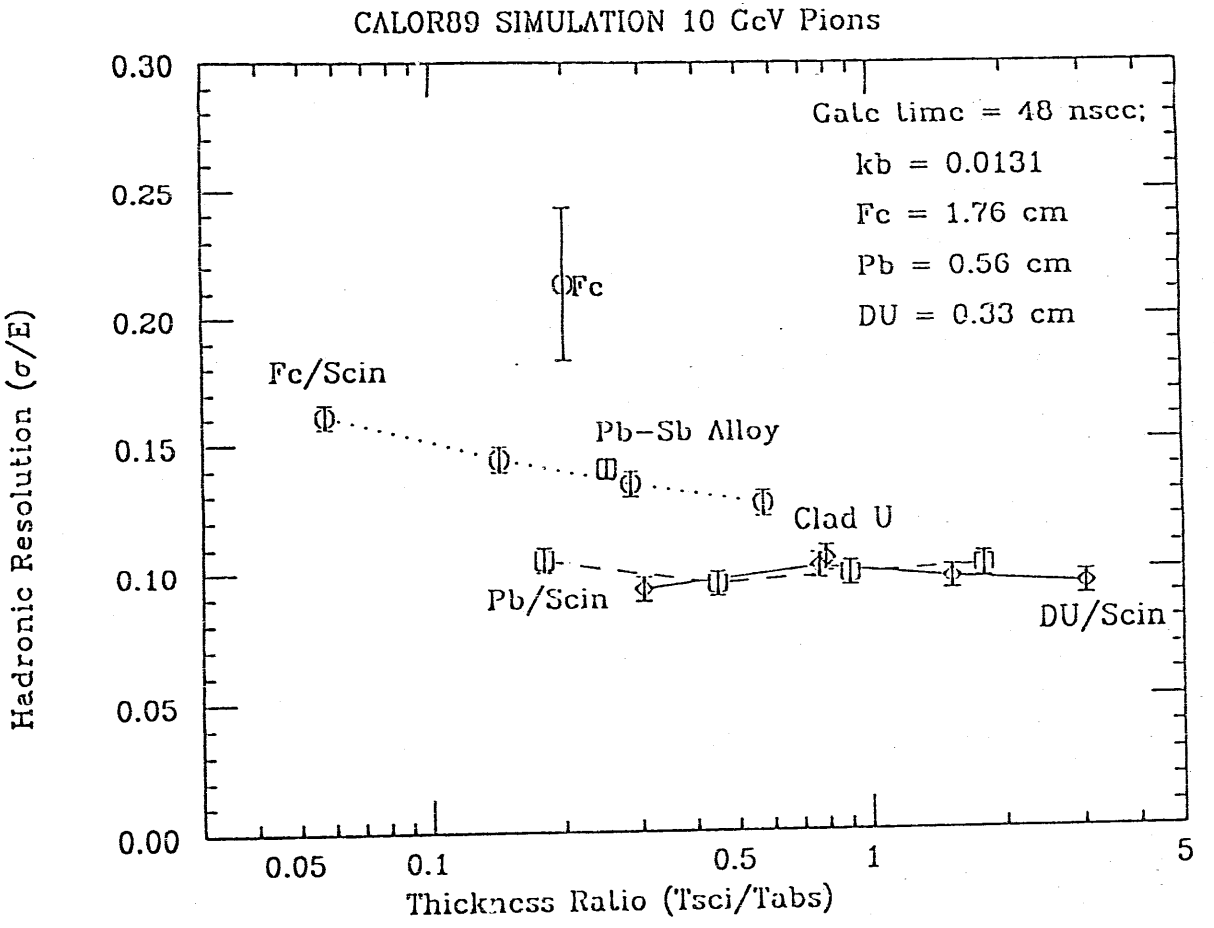


Fig. 10(b) Hadronic energy resolution as a function of scintillator thickness divided by a fixed thickness of absorber.

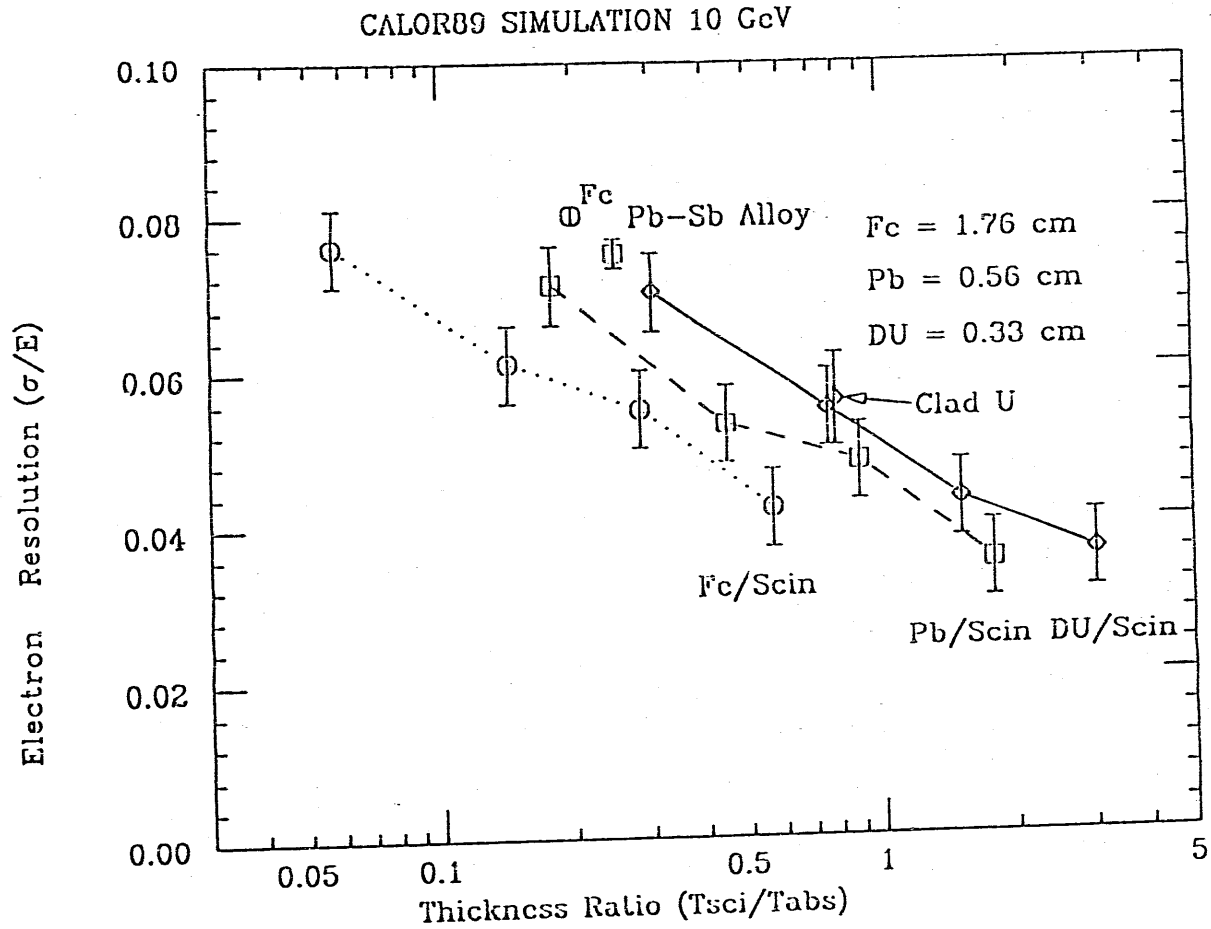


Fig. 11(a) Electromagnetic energy resolution as a function of absorber thickness divided by a fixed thickness of scintillator.

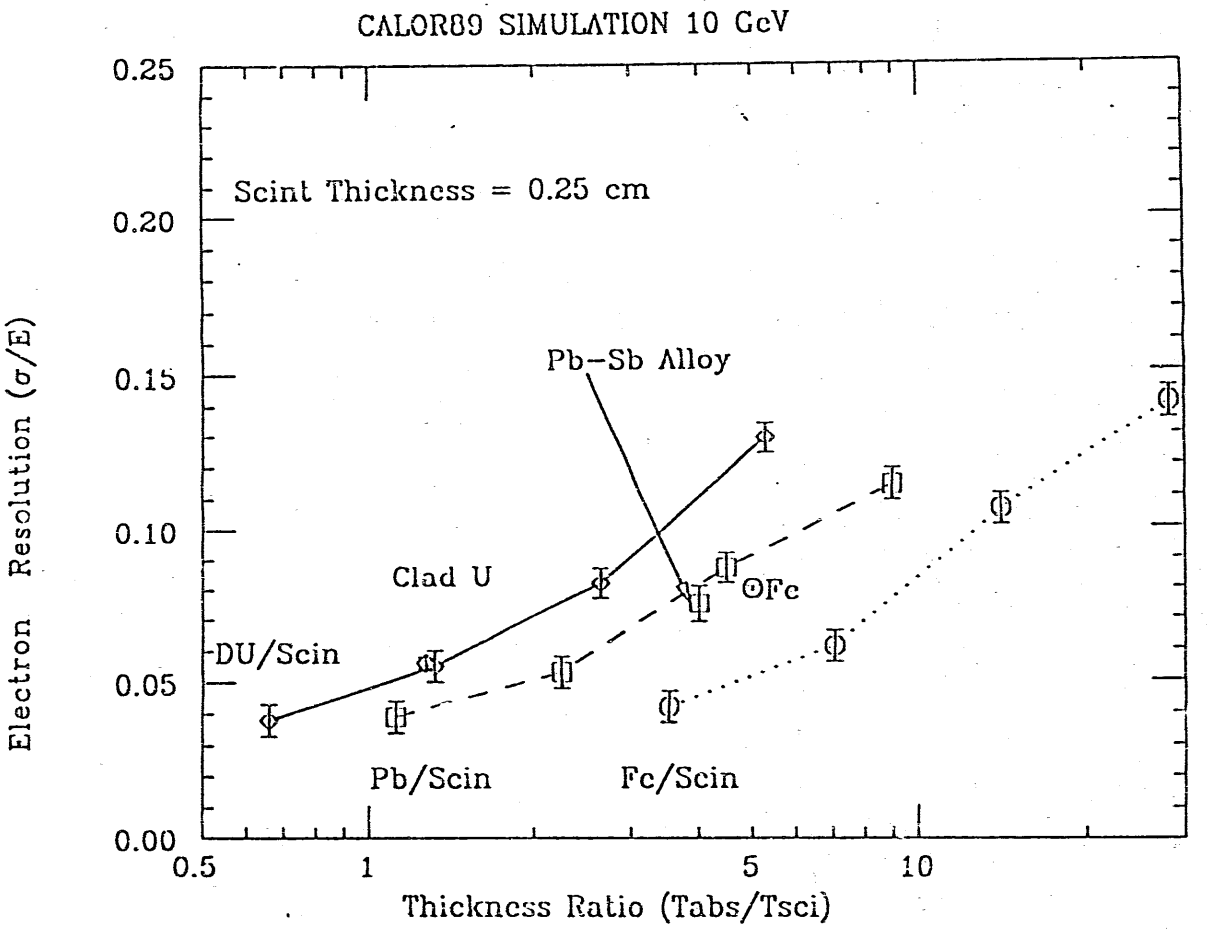


Fig. 11(b) Electromagnetic energy resolution as a function of scintillator thickness divided by a fixed thickness of absorber.

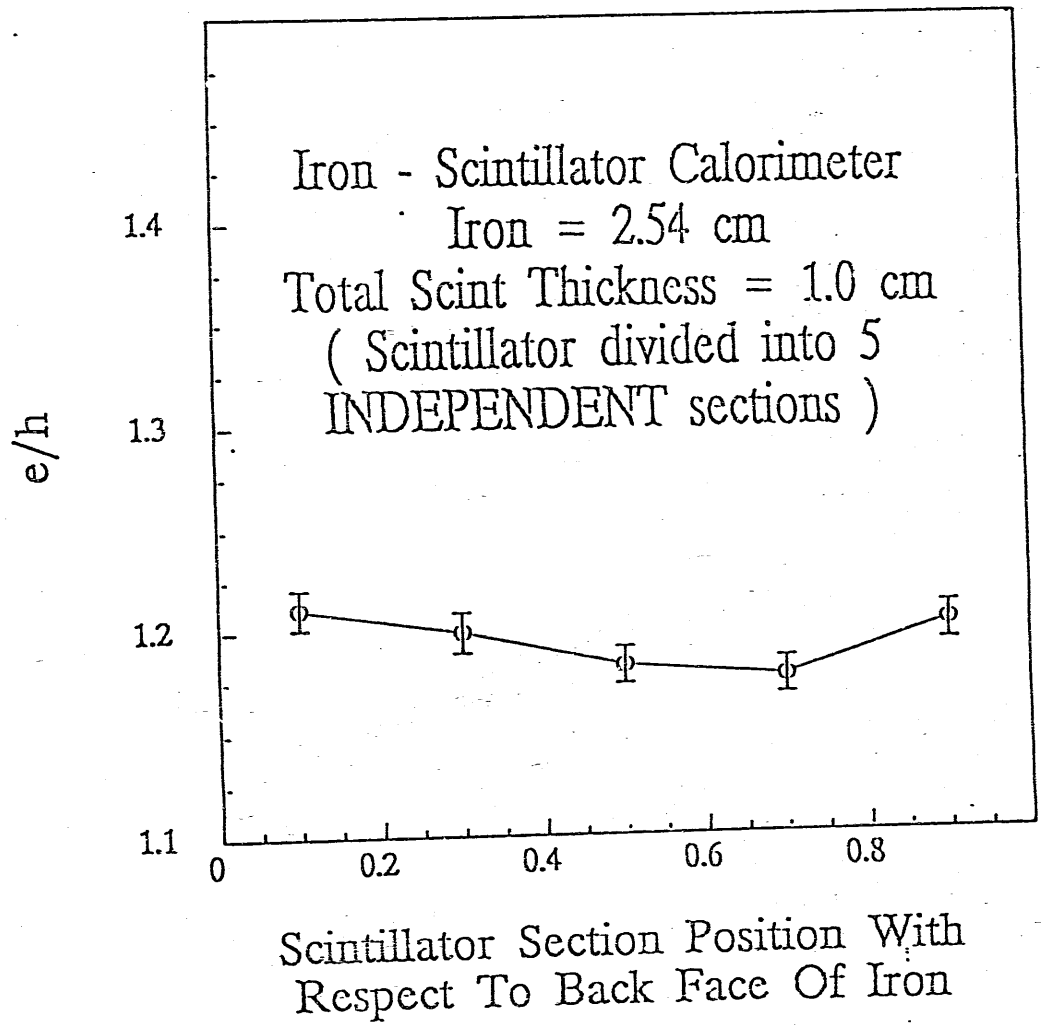


Fig. 12 Compensation at 10 GeV for various layers of plastic scintillator. Each section is independent.

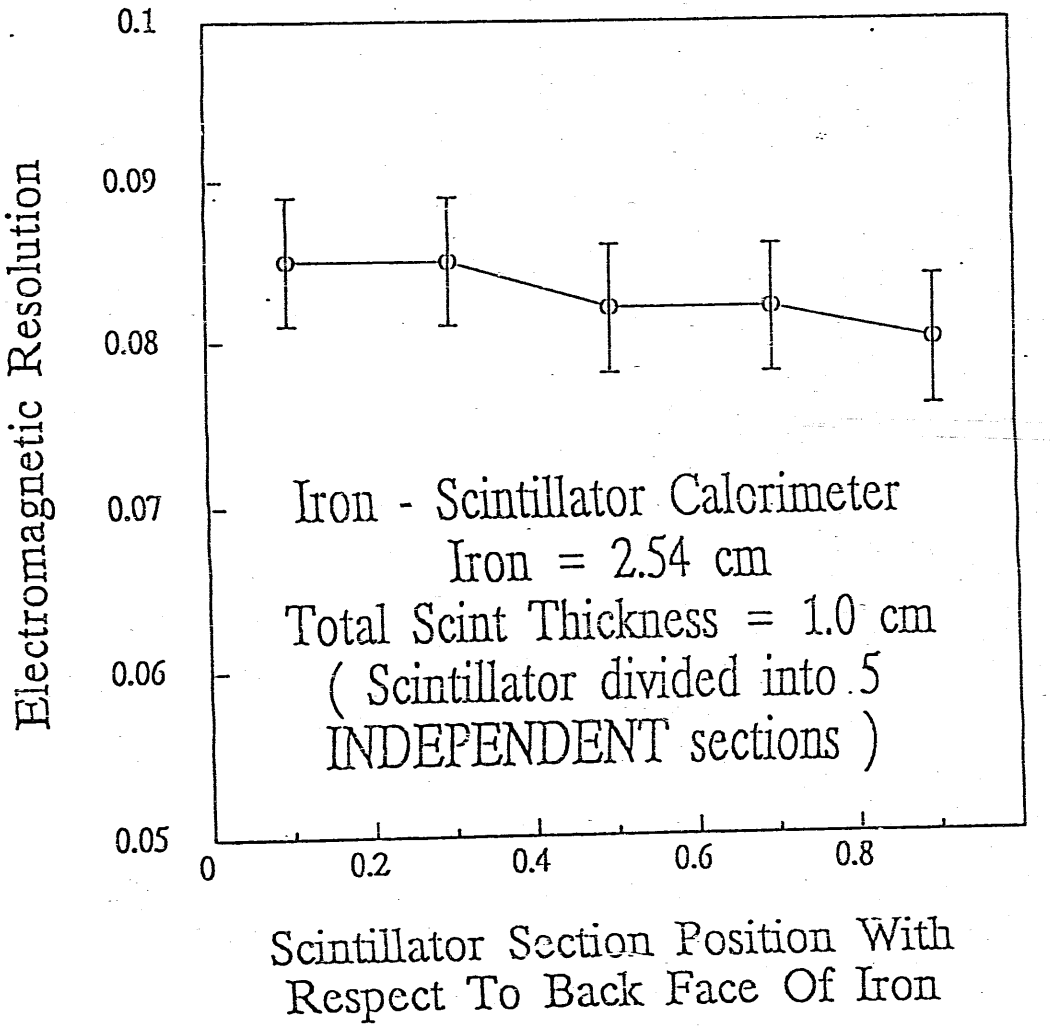


Fig. 13 **Electromagnetic energy resolution at 10 GeV for various layers of plastic scintillator. Each section is independent.**

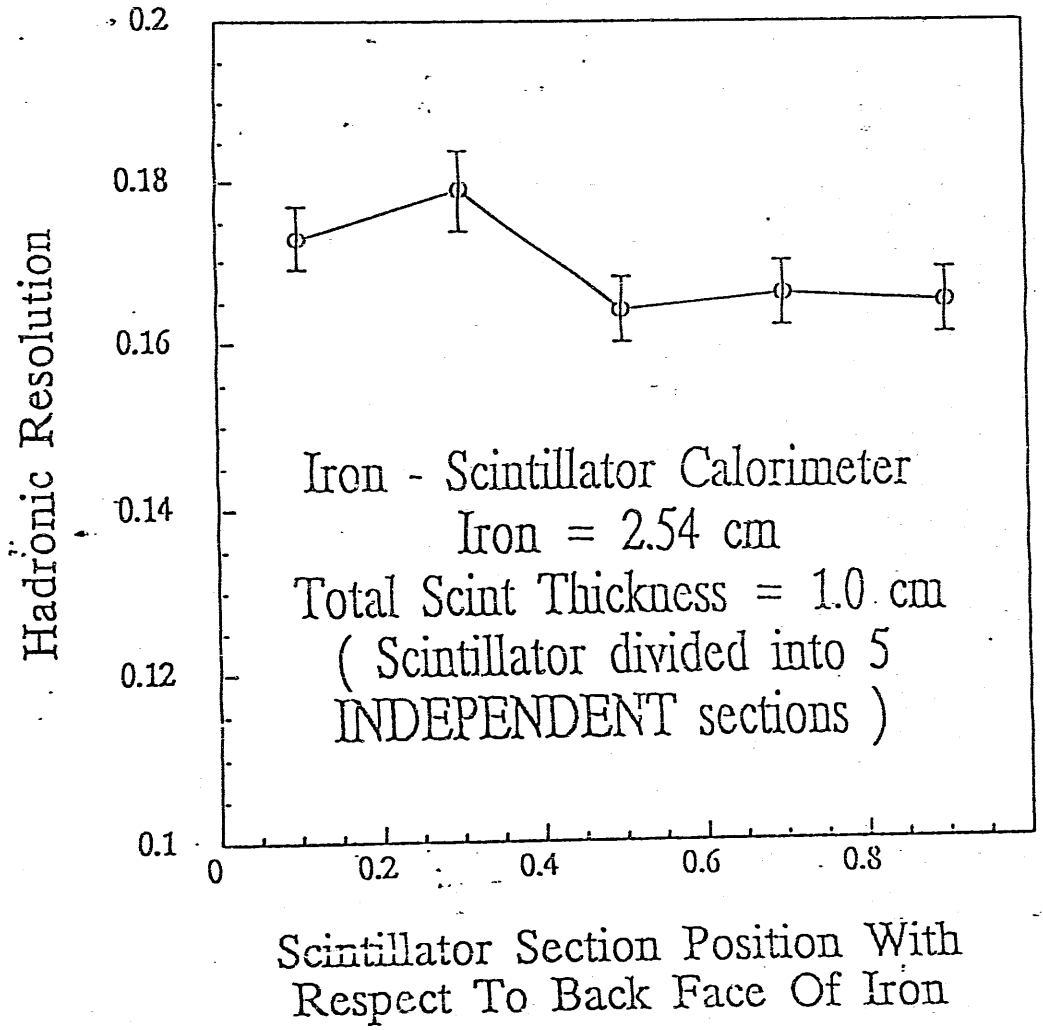


Fig. 14 Hadronic energy resolution at 10 GeV for various layers of plastic scintillator. Each section is independent.

## 6. References

1. J. Brau and T. A. Gabriel, NIM 238, 489 (1985). T. A. Gabriel, et al., IEEE Trans. Nucl. Sci. NS-32, 1 (1985), and references contained therein.

2. R. G. Alsmiller, Jr., F. S. Alsmiller, and O. W. Hermann, "The High Energy Transport Code - HETC88 and Comparison with Experimental Data," submitted to Nucl. Inst. & Meth.

3. W. R. Nelson, et al., SLAC-265, Stanford Linear Accelerator Center, (1985).

4. M. B. Emmett, ORNL-4972, Oak Ridge National Laboratory, (1975). N. M. Greene, et al., ORNL/TM-3706, Oak Ridge National Laboratory, (1973).

5. J. O. Johnson and T. A. Gabriel, ORNL/TM-10196, Oak Ridge National Laboratory, (1987).

6. H. W. Bertini, Phys. Rev. 188(1969)1711.

7. J. Ranft and S. Ritter, Z Phys. C: Part. Fields 10(1989)249. P. A. Aarnio, et al., "CERN TIS Divisional Report," TIS-RP/106-Rev., 1984. A. Capella and J. Tran Thanh Van., Phys. Letts., 938(1980)2.

8. J. B. Birks, Proc. Phys. Soc., A64(1951)874.

9. H. Abrahamowics, et al., Nucl. Inst. & Meth. 180(1980)429.

10. E. Bernardi, et al., Nucl. Inst. & Meth., A262(1987)229.

11. E. Ros and T. Tsurugai, ZEUS Note 88-086(1988).

12. M. Abolins, et al., Nucl. Inst. & Meth., A280(1987)36.

13. S. Aronson, et al., NIM A269(1988)492.

# END

# DATE FILMED

02 / 07 / 91